Finite-size scaling at first-order quantum transitions when boundary conditions favor one of the two phases

Andrea Pelissetto,[1] Davide Rossini,[2] and Ettore Vicari[2,*]

[1]*Dipartimento di Fisica dell'Università di Roma "La Sapienza" and INFN, Sezione di Roma I, I-00185 Roma, Italy*

[2]*Dipartimento di Fisica dell'Università di Pisa and INFN, Largo Pontecorvo 3, I-56127 Pisa, Italy*

(Received 29 June 2018; published 20 September 2018)

We investigate scaling phenomena at first-order quantum transitions, when the boundary conditions favor one of the two phases. We show that the corresponding finite-size scaling behavior, arising from the interplay between the driving parameter and the finite size of the system, is more complex than that emerging when boundary conditions do not favor any phase. We discuss this issue in the framework of the paradigmatic one-dimensional quantum Ising model, along its first-order quantum transition line driven by an external longitudinal field. Specifically, three regions with distinct scaling behaviors emerge, which correspond to different values of the field (small, intermediate, and large field), according to its capability to modify the phase favored by the boundary conditions.

DOI: 10.1103/PhysRevE.98.032124

I. INTRODUCTION

Zero-temperature quantum phase transitions are phenomena of great interest [1–3]. They arise in many-body systems with competing ground states controlled by nonthermal parameters. They are continuous when the ground state of the system changes continuously at the transition point and correlation functions develop a divergent length scale. They are instead of first order when ground-state properties are discontinuous across the transition point. In general, singularities develop only in the infinite-volume limit. If the size L of the system is finite, then all properties are analytic as a function of the external parameter driving the transition. However, around the transition point, low-energy thermodynamic quantities and large-scale structural properties show a finite-size scaling (FSS) behavior depending only on the general features of the transition. An understanding of these finite-size properties is important for a correct interpretation of experimental or numerical data, when phase transitions are investigated in relatively small systems—see, e.g., Refs. [4–9]. These issues cover a fundamental role also at first-order quantum transitions (FOQTs), which are very interesting, as they occur in a large number of quantum many-body systems, such as quantum Hall samples [10], itinerant ferromagnets [11], heavy fermion metals [12–14], etc.

Crossings of the lowest-energy states give rise to FOQTs. In the absence of conservation laws, they only occur in the infinite-volume limit [15]. In a finite system, the presence of a nonvanishing matrix element among these states lifts the degeneracy, giving rise to the phenomenon of avoided level crossing. The emerging FSS behaviors have been mostly investigated [9,16–19] assuming boundary conditions that do not favor any of the different phases at the FOQT. Here we are going to extend the discussion to boundary conditions that favor one of the two phases.

Understanding the FSS behavior of quantum many-body systems in the presence of various types of boundary conditions is worth being examined in depth, not only from a theoretical point of view. As a matter of fact, experimentally realistic situations generally deal with boundary conditions that are different from the periodic ones (which are routinely employed in FSS studies). For example, boundary conditions analogous to those considered here can be enforced by considering molecular spin wires with each boundary coupled to a magnetic impurity [20]. On the other hand, the outstanding developments in the field of ultracold atomic and molecular optics recently enabled to confine such systems in box-shaped traps [21], thus paving the way toward an accurate control of the boundary conditions, beyond the standard harmonic confinement.

In this paper we study the role of boundary conditions favoring one of the two phases in the context of the simplest paradigmatic quantum many-body system, exhibiting a nontrivial zero-temperature behavior: the one-dimensional quantum Ising chain in the presence of a transverse field. Its zero-temperature phase diagram presents a line of FOQTs driven by a longitudinal external field. Earlier works [9,17–19] considered boundary conditions that are invariant under the $\mathbb{Z}_2$ spin-inversion symmetry and which therefore do not favor any of the two phases—they will be called neutral boundary conditions henceforth; for instance, periodic, antiperiodic, or open boundary conditions (PBC, ABC, and OBC, respectively). As we shall see, the FSS emerging when boundary conditions favor one of the two magnetized phases, substantially differs from, and appears more complex than, those already found for neutral boundary conditions. Specifically, we consider equal fixed boundary conditions (EFBC), with both boundary states favoring the same phase. We locate three distinct regions corresponding to different values of the longitudinal field h. A very small field cannot modify

[*]Authors are provided in alphabetical order.

the system's phase stabilized by the EFBC, and observables smoothly depend on it. Conversely, for intermediate fields around a transition value $h_{\rm tr} \sim 1/L$, the interplay between the boundary conditions and the field drives a FOQT with a universal FSS behavior dictated by the competition of the two exponentially close lowest-energy states. Finally, larger longitudinal fields are able to fix the bulk phase; here we find another peculiar scaling behavior, which is controlled by a different variable.

This paper is organized as follows. In Sec. II we introduce the one-dimensional quantum Ising model and some of the observables which are interesting to be considered along the FOQT line driven by the longitudinal field. Moreover, we summarize the relevant features of the FSS behavior in the presence of neutral boundary conditions, such as PBC, OBC, and ABC. Section III reports the main results of this research, i.e., the numerical study of the finite-size quantum Ising chain with EFBC favoring one of the two magnetized phases. Finally, in Sec. IV we draw our conclusions and perspectives.

II. THE QUANTUM ISING CHAIN

A. Model and its observables

The quantum Ising chain in a transverse field is perhaps the simplest quantum many-body system exhibiting a nontrivial zero-temperature phase diagram. The corresponding Hamiltonian, in the presence of an additional longitudinal field, reads

$$H_{\rm Is} = -J \sum_{\langle x,y\rangle} \sigma_x^{(3)}\sigma_y^{(3)} - g \sum_x \sigma_x^{(1)} - h \sum_x \sigma_x^{(3)}, \qquad (1)$$

where $\boldsymbol{\sigma} \equiv [\sigma^{(1)}, \sigma^{(2)}, \sigma^{(3)}]$ are the Pauli matrices, the first sum is over all bonds of the chain connecting nearest-neighbor sites $\langle x, y\rangle$, while the other sums are over the L sites of the chain. We assume $\hbar = 1$, $J = 1$, and $g > 0$.

At $g = 1$ and $h = 0$, the model undergoes a continuous quantum transition (CQT) belonging to the two-dimensional Ising universality class, separating a disordered phase ($g > 1$) from an ordered ($g < 1$) one [2]. For any $g < 1$, the field h drives FOQTs along the $h = 0$ line. We are interested in the FSS behavior of the system along the FOQT line, i.e., in the interplay between the longitudinal field h and the size L, for $g < 1$.

In a FOQT, low-energy properties depend on the chosen boundary conditions, even in the limit $L \to \infty$. If one considers neutral boundary conditions, then the behavior close to the transition can be completely characterized by considering two magnetized states $|+\rangle$ and $|-\rangle$ such that [22]

$$\langle \pm|\sigma_x^{(3)}|\pm\rangle = \pm m_0, \qquad m_0 = (1-g^2)^{1/8}, \qquad (2)$$

in the infinite-volume limit. Moreover, the longitudinal average magnetization

$$m(L,h) = \frac{1}{L}\sum_x \langle \sigma_x^{(3)}\rangle, \qquad (3)$$

is discontinuous, i.e., $\lim_{h\to 0^\pm} \lim_{L\to\infty} m(L,h) = \pm m_0$. We should, however, note that this simple two-level description does not hold for some other choices of boundary conditions, as we discuss below.

Here we are going to investigate the finite-size behavior of the energy difference $\Delta(L,h)$ of the lowest-energy states,

$$\Delta(L,h) \equiv E_1(L,h) - E_0(L,h), \qquad (4)$$

the average magnetization $m(L,h)$ defined in Eq. (3), and the local magnetization $m_c(L,h)$ at the center of the chain,

$$m_c(L,h) = \langle \sigma_{x_c}^{(3)}\rangle, \qquad (5)$$

where x_c is the central site of the chain (or one of the two central sites, when L is even). Let us also introduce the renormalized average and central magnetizations

$$M = \frac{m}{m_0}, \quad M_c = \frac{m_c}{m_0}, \qquad (6)$$

which take the values ± 1, in the limit $L \to \infty$, for $h \to 0^\pm$ and any $g < 1$.

The FSS behaviors originating from the cases of neutral boundary conditions have been already scrutinized in earlier works [9,17]. In order to appreciate the new emerging features of FSS for boundary conditions favoring one of the two magnetized phases, it is instructive to first briefly summarize the known features of FSS for neutral boundary conditions. This is the purpose of the remainder of this section. The next section reports the results of our analysis, dealing with EFBC favoring one of the two magnetized phases.

B. Finite-size scaling with periodic and open boundary conditions

In a finite system of size L with PBC or OBC, due to tunneling effects, the lowest eigenstates are superpositions of the states $|+\rangle$ and $|-\rangle$, defined as $\langle \pm|\sigma_x^{(3)}|\pm\rangle = \pm m_0$. For $h = 0$, their energy difference

$$\Delta_0(L) \equiv \Delta(L, h = 0) \qquad (7)$$

vanishes exponentially as L increases [22,23]:

$$\Delta_0(L) = 2\,(1-g^2) g^L\,[1 + O(g^{2L})] \quad \text{for OBC}, \qquad (8)$$

$$\Delta_0(L) \approx 2\,\sqrt{(1-g^2)/(\pi L)}\, g^L \qquad \text{for PBC}. \qquad (9)$$

On the other hand, the difference $\Delta_{0,i} \equiv E_i - E_0$ for the higher excited states ($i > 1$) remains finite for $L\to\infty$, in particular $\Delta_{0,2} = 2(1-g) + O(L^{-2})$ for OBC and $\Delta_{0,2} = 4(1-g) + O(L^{-2})$ for PBC.

The interplay between the size L and the field h gives rise to an asymptotic FSS of the low-energy properties [9], in particular those related to the ground state. The relevant scaling variable is the ratio between the energy associated with the longitudinal field h, i.e., $2m_0hL$, and the gap $\Delta_0(L)$ at $h = 0$,

$$\kappa = \frac{2m_0 h L}{\Delta_0(L)}. \qquad (10)$$

The FSS limit corresponds to $L \to \infty$ and $h \to 0$, keeping κ fixed. In this limit, the gap Δ and the magnetization behave as

$$\Delta(L,h) \approx \Delta_0(L)\,\mathcal{D}(\kappa), \qquad (11)$$

$$M(L,h) \approx M_c(L,h) \approx \mathcal{M}(\kappa). \qquad (12)$$

Note—this remark will be important in the case of EFBC—that the energy $2m_0hL$ can be interpreted as the difference between the magnetic energy at the given value of h and that at the value where the gap displays its minimum, i.e., for $h = 0$.

In the PBC and OBC cases, the scaling functions can be exactly computed. Since, close to the FOQT, the low-energy spectrum is characterized by the crossing of the two lowest levels, while the energy differences $\Delta_{0,i}$ with the other ones remain finite, FSS functions can be obtained by performing a two-level truncation [9,24], keeping only the two lowest energy levels $|\pm\rangle$. Then, a straightforward calculation leads to the scaling functions

$$\mathcal{D}(x) = \mathcal{D}_{2l}(x) = \sqrt{1+x^2}, \tag{13}$$

$$\mathcal{M}(x) = \mathcal{M}_{2l}(x) = \frac{x}{\sqrt{1+x^2}}. \tag{14}$$

It is important to note that, in the derivation of Eq. (14), we have assumed that the magnetization M of the two states $|\pm\rangle$ is ± 1, respectively.

It is also worth mentioning that an analogous FSS behavior emerges when, instead of the homogeneous field h, we consider an external longitudinal field h_l applied at one site only [9,24]. The only difference amounts to replacing the product hL with h_l in the definition (10) of the scaling variable κ, while the two-level truncation holds as well. In a sense, the system behaves rigidly at the FOQT when PBC or OBC are considered, i.e., its response to global or local longitudinal perturbations is analogous.

C. Finite-size scaling with antiperiodic boundary conditions

The size dependence of the gap $\Delta_0(L)$ at FOQTs may significantly depend on the boundary conditions, exhibiting a power-law behavior in some cases [9,17,23,25]. For example, for ABC [17] we have

$$\Delta_0(L) \equiv \Delta(L, h=0) = \frac{g}{1-g}\frac{\pi^2}{L^2} + O(L^{-4}). \tag{15}$$

This is related to the fact that the low-energy states for ABC are one-kink states (characterized by a nearest-neighbor pair of antiparallel spins), which behave as one-particle states with $O(L^{-1})$ momenta. Therefore, using Eq. (10), we expect FSS to hold if we define the scaling variable κ as

$$\kappa \sim hL^3. \tag{16}$$

Such a behavior has been indeed observed in Ref. [9]. However, in this case, scaling functions cannot be obtained by performing a two-level truncation, because the low-energy spectrum at the transition point presents a tower of excited stated with $\Delta_{0,i} = O(L^{-2})$, at variance with the OBC and PBC case, where only two levels matter, close to the transition point.

Note that a similar behavior also emerges for fixed and opposite boundary conditions [17], for which the lowest states can be associated with kink states, as well.

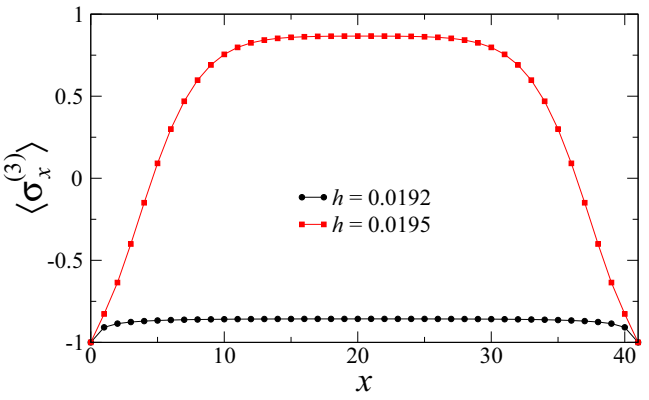

FIG. 1. Magnetization profile along the magnetic-field direction in the presence of EFBC, for $L = 40$, $g = 0.8$, and two values of the longitudinal field h. Note that the local magnetization for $x = 0$ and $x = L + 1 = 41$ is exactly -1, because of the boundary conditions.

III. BOUNDARY CONDITIONS FAVORING ONE OF THE TWO PHASES

Let us now focus on a quantum Ising chain of size L with EFBC favoring one of the two magnetized phases. We consider $L + 2$ spins defined at the lattice sites $x = 0, \ldots, L + 1$ and the Hamiltonian

$$H_{\rm Is} = -\sum_{x=0}^{L} \sigma_x^{(3)}\sigma_{x+1}^{(3)} - g\sum_{x=1}^{L}\sigma_x^{(1)} - h\sum_{x=1}^{L}\sigma_x^{(3)}. \tag{17}$$

EFBC are fixed by restricting the Hilbert space to states $|s\rangle$ such that $\sigma_0^{(3)}|s\rangle = -|s\rangle$ and $\sigma_{L+1}^{(3)}|s\rangle = -|s\rangle$.

As we shall see below, the interplay between the size L and the bulk longitudinal field h gives rise to a more complex finite-size behavior, with respect to that of neutral boundary conditions. In the following, this issue is investigated by analyzing numerical results for two values of g, i.e., $g = 0.5$ and $g = 0.8$, obtained by exact diagonalization, up to $L \approx 22$, and density-matrix renormalization group (DMRG) methods [26] for larger sizes, up to $L \approx 300$ [27].

EFBC can be naturally enforced with exact methods. On the other hand, DMRG naturally works with OBC. Therefore, in this case we effectively simulated a nonhomogeneous chain of $L + 2$ sites with OBC, and then added two large local magnetic fields on the first and last site, whose net effect is that of removing from the low-energy spectrum the unwanted states, i.e., those corresponding to $|\uparrow\rangle$ occupancies in the two boundary sites [27].

Before entering the details of our discussion, let us provide a qualitative picture of the system's response to the longitudinal field h, by analyzing the magnetization profile. Figure 1 highlights the net macroscopic effect of two values of h, on a system with $L = 40$ sites, $g = 0.8$, and EFBC. It emerges that, if the longitudinal field is not sufficiently strong, the magnetization profile displays a nearly flat behavior: because of the boundary conditions, the value of $\langle\sigma_x^{(3)}\rangle$ always stays close to -1, corresponding to the $|\downarrow\rangle$ state on each site x of the chain. Conversely, a sufficiently large value of h is able to substantially modify the profile, inducing a local magnetization in the bulk of the chain which is close to $+1$

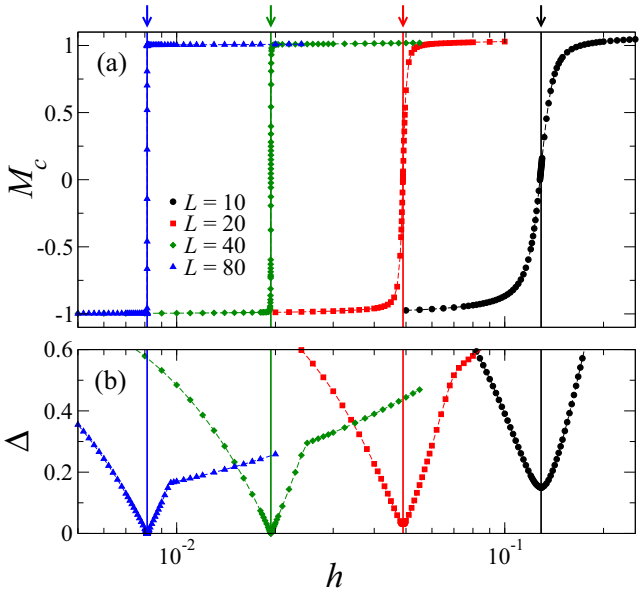

FIG. 2. Central magnetization M_c (a) and energy gap Δ (b) in the Ising model with EFBC, as a function of the longitudinal field h, for fixed transverse field $g = 0.8$. The various data sets correspond to different system sizes, as indicated in the legend. The continuous vertical lines and arrows denote the magnetic fields $h_{\rm tr}(L)$, which correspond to the minimum of the energy gap, as displayed in panel (b).

(corresponding to a $|\uparrow\rangle$ state), thus opposed to that favored by the EFBC. Thus, there should exist some threshold value (or region) of h, separating the two distinct behaviors.

A glimpse at the numerical data of the central magnetization M_c versus h presented in Fig. 2(a) immediately spotlights that the above outlined transition from $M_c \approx -1$ to $M_c \approx +1$ is indeed very rapid, when increasing h across an L-dependent value $h_{\rm tr}(L) > 0$ (indicated with arrows and continuous vertical lines in the figure), which approaches $h = 0$ when increasing L. While for small sizes we observe a smooth crossover between the two phases, this crossover becomes sharper when increasing L, until we are not able to distinguish the transition region (see the results for $L = 80$ in the figure). The transition region also shrinks if we fix L and consider a transverse field g farther from $g = 1$. This sharp crossover corresponds to the minimum $\Delta_m(L)$ of the energy difference of the two lowest states, see Fig. 2(b), evidencing the correspondence with an avoided level crossing, where the energies of such two states get closer and closer with increasing L. Actually, we may define $h_{\rm tr}(L)$ as the value of h where the gap shows its minimum, $\Delta_m(L) \equiv \Delta[L, h_{\rm tr}(L)]$, which vanishes in the thermodynamic limit $L \to \infty$.

We stress that the minimum of the energy gap, that we can interpret as the finite-size pseudotransition point, is located at $h_{\rm tr}(L) > 0$, at variance with what occurs for neutral boundary conditions, where the minimum is always located at $h = 0$ for any value of L.

Summarizing, we can identify three distinct regions, corresponding to (a) small values of h, where the longitudinal field ($h < h_{\rm tr}$) is unable to modify the phase of the system stabilized by the EFBC; (b) intermediate values of h around $h_{\rm tr}(L)$, where the interplay between the boundary conditions and the field induces a sharp transition; (c) large values of h, where the bulk phase is determined by the field ($h > h_{\rm tr}$). Below we separately discuss the emerging physics in these three regions.

A. Small-h region

For $h = 0$, the phase with negative magnetization is favored by the boundary conditions. Correspondingly, we have

$$\lim_{L\to\infty} M(L, 0) = \lim_{L\to\infty} M_c(L, 0) = -1, \tag{18}$$

and the gap is finite [19]:

$$\Delta_0(L) = 4(1 - g) + O(L^{-2}). \tag{19}$$

The finite-size transition to the phase with positive magnetization occurs for $h \approx h_{\rm tr}(L) > 0$. Therefore, at fixed L, we expect observables to be smooth for $h \approx 0$ and to have a regular expansion around $h = 0$, which is predictive up to $h_{\rm tr}(L) > 0$. The L dependence of the observables in this regime depends on their nature. Local observables that are defined far from the boundaries (they are localized in a region whose distance from the boundaries is much larger than the correlation length ξ of the system) are expected to have a negligible dependence on L, thus they smoothly depend only on h, for $h < h_{\rm tr}(L)$. In particular, this is the case for the central magnetization M_c: when $L \gg \xi$ and $h < h_{\rm tr}(L)$, $M_c \approx f_m(h)$, with a little dependence on L. This agrees with our numerical findings (data not shown here). On the other hand, the energy gap, which is a global quantity, obeys the scaling relation

$$\Delta(L, h) \approx \Delta_0(L)\, f_\Delta(hL), \tag{20}$$

where $f_\Delta(x)$ is a smooth function of x, around $x = 0$. This is shown in Fig. 3, where we clearly observe data collapse for $g = 0.5$ already at small sizes (main frame), while for $g = 0.8$ the collapse occurs at larger sizes (inset). The slower approach to scaling when raising g along the FOQT line can be easily explained by the increasing correlation length $\xi \sim (1 - g)^{-1}$, when approaching the CQT at $g = 1$.

B. Transition region

For $h \approx h_{\rm tr}(L)$, the gap between the ground state and the first excited state becomes small. We were able to reliably determine its minimum $\Delta_m(L)$ up to values of the order of 10^{-6}, within the accuracy of our numerical simulations—see Fig. 4. Our data show that $\Delta_m(L) \sim e^{-bL}$ for L sufficiently large. We estimate $b \approx 0.481$ and $b \approx 0.15$, for $g = 0.5$ and $g = 0.8$, respectively.

The position of $h_{\rm tr}(L)$ can be determined more accurately, since its estimate does not require to probe regions with very small gaps, where numerical methods, such as Lanczos or DMRG, may typically encounter problems. Using DMRG, we obtained results up to $L = 300$, as shown in Fig. 5. The resulting estimates of $h_{\rm tr}(L)$ are very accurate. In particular, the relative accuracy is of the order of 10^{-6} for $g = 0.5$ ($L \gtrsim 100$) and of 10^{-4} for $g = 0.8$. Results are consistent with the expected $1/L$ asymptotic behavior, i.e.,

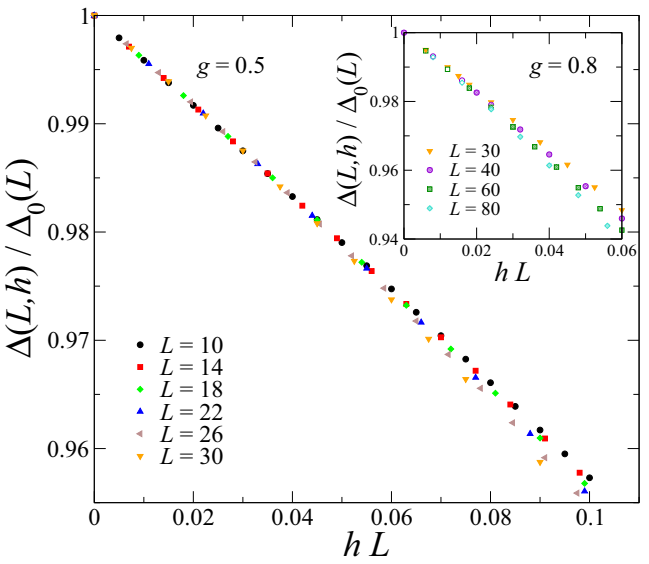

FIG. 3. Energy gap ratio $\Delta(L,h)/\Delta_0(L)$ as a function of the rescaled variable hL, for $g = 0.5$ (main frame) and for $g = 0.8$ (inset). The symbols correspond to different values of L.

with

$$\lim_{L\to\infty} L\, h_{\rm tr}(L) = \eta, \tag{21}$$

where η decreases with g. However, the next-to-leading corrections are not consistent with the expected analytic $1/L^2$ behavior. Our data indicate $L\, h_{\rm tr}(L) = \eta + O(L^{-\zeta})$, where ζ is an exponent that is strictly less than 1 (see the inset of Fig. 5). For both $g = 0.5$ and $g = 0.8$, the data for the largest sizes are consistent with the ansatz

$$L\, h_{\rm tr} = \eta + a_1 L^{-\zeta} + a_2 L^{-1} \tag{22}$$

with $\zeta \approx 2/3$ (the L^{-1} term represents an analytical corrections which must be generally present). If we fit our data for $g = 0.5$ and $L \geqslant 100$ to the ansatz (22), then we obtain

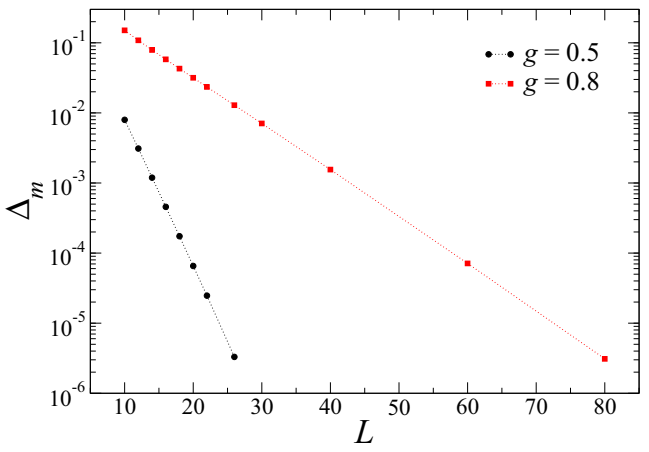

FIG. 4. Minimum gap Δ_m for $h = h_{\rm tr}(L)$ as a function of the system size L, for two different values of g, as explained in the legend. The dotted lines are only meant to guide the eye: They show that the data approximately behave as $\Delta_m \sim e^{-bL}$.

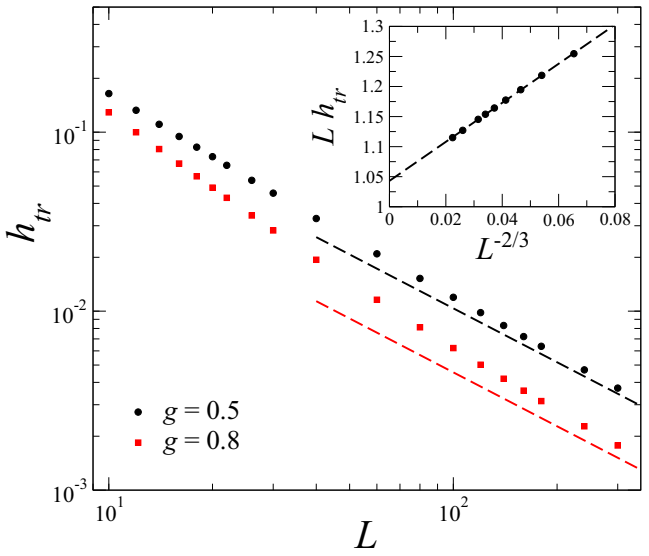

FIG. 5. Longitudinal-field value $h_{\rm tr}(L)$ at which the system exhibits a minimum in the gap, as a function of the size L, for two different values of g, as explained in the legend. The dashed lines correspond to the asymptotic behavior $h_{\rm tr}(L) \approx \eta/L$, cf. Eq. (21). The inset displays $L\, h_{\rm tr}(L)$ for $g = 0.5$, as a function of $L^{-2/3}$: Data fall on a straight line, showing the presence of corrections of order $L^{-2/3}$. The uncertainty on the estimates of $h_{\rm tr}(L)$ is always smaller than the symbols sizes.

$\eta = 1.0370(5)$, $a_1 = 4.0(1)$, and $\zeta = 0.67(1)$ with $\chi^2/{\rm dof} \approx 1$ (dof is the number of degrees of freedom of the fit and χ^2 is the sum of the residuals). Errors are estimated by also taking into account the variation of the results with the minimum size allowed in the fit. Analogously, for $g = 0.8$, fitting the available data for $L \gtrsim 60$ gives $\eta = 0.455(5)$, $a_1 = 2.6(6)$, and $\zeta = 0.64(4)$, with $\chi^2/{\rm dof} \lesssim 0.5$. We will return to this point later, in Sec. III C, providing an explanation for the $O(L^{-\zeta})$ correction with $\zeta = 2/3$ in Eq. (22).

The above picture, and in particular the asymptotic behavior of $h_{\rm tr}(L)$, is also supported by the analysis of the $g \to 0$ limit, where the energy levels of model (17) can be easily computed, obtaining that $h_{\rm tr}(L) = 2/L$, thus $\eta = 2$, in the limit $g \to 0$. In this limit, it is also trivial to verify that that gap Δ_m at $h_{\rm tr}(L)$ decreases exponentially as e^{-bL} with $b \approx -\ln g$.

For h close to $h_{\rm tr}(L)$, we can define a FSS in terms of the scaling variable

$$y = \frac{2m_0 L\,[h - h_{\rm tr}(L)]}{\Delta_m(L)}\,. \tag{23}$$

This variable is the analog of κ defined in Eq. (10). The essential difference is related to the fact that the finite-size pseudotransition occurs at $h = h_{\rm tr}(L)$, and not at $h = 0$. Therefore, the relevant magnetic energy scale is the difference between the magnetic energy at h and that at $h_{\rm tr}(L)$, while the relevant gap is the one at $h_{\rm tr}(L)$. The infinite-volume critical point $h = 0$ lies outside the region in which FSS holds. Note that a crucial point in the definition of the scaling variable y is that the values of $h_{\rm tr}(L)$ and $\Delta_m(L)$ must be those associated with the minimum of the gap for the given size L, i.e., they cannot be replaced with their asymptotic behaviors.

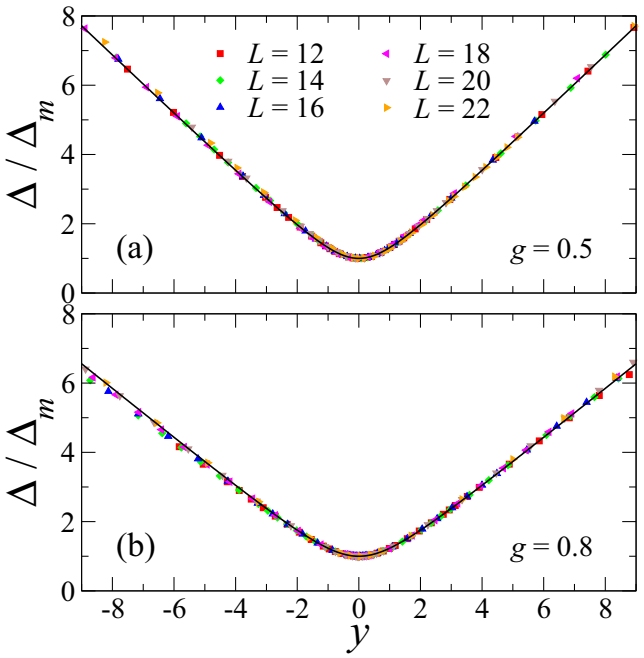

FIG. 6. Ratio Δ/Δ_m, where $\Delta \equiv \Delta(L,h)$ is the gap and $\Delta_m \equiv \Delta(L,h_{\rm tr})$, as a function of the scaling variable y defined in Eq. (23), for several system sizes (see the legend). Panel (a) is for $g = 0.5$, while panel (b) is for $g = 0.8$. We also report (continuous black curve) the two-level prediction (27).

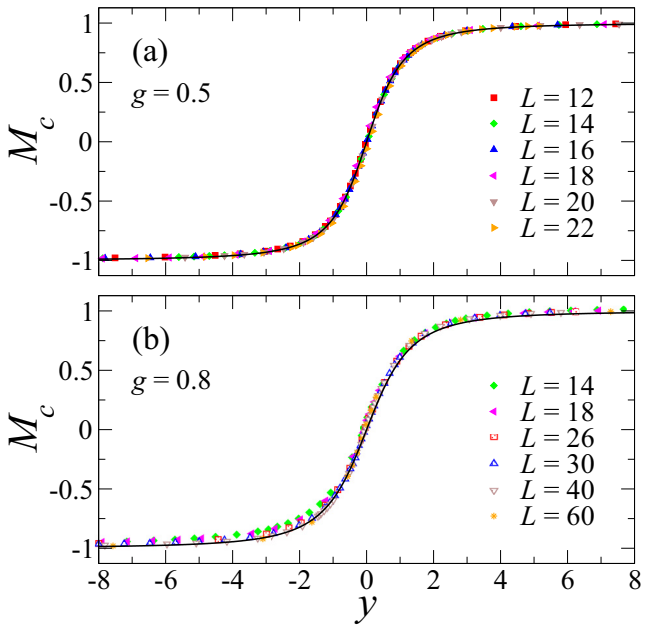

FIG. 7. Local magnetization at the center of the chain M_c, as a function of the scaling variable y, for several system sizes (see the legend). Panel (a) is for $g = 0.5$, while panel (b) is for $g = 0.8$. We also report (continuous black curve) the two-level prediction (28), with the same constant c as in Fig. 6.

For $h \approx h_{\rm tr}(L)$, observables are expected to develop a FSS behavior given by

$$\Delta(L,h) \approx \Delta_m(L)\, \mathcal{D}_f(y), \tag{24}$$

$$M_c(L,h) \approx \mathcal{M}_{cf}(y), \tag{25}$$

$$M(L,h) \approx \mathcal{M}_f(y). \tag{26}$$

These predictions are nicely supported by the data, see Figs. 6, 7, and 8. We observe that the convergence to the asymptotic infinite-volume limit appears to be slightly slower for $g = 0.8$, as is reasonable for values of the transverse field which are closer to $g = 1$ [this is especially evident in panel (b) of Fig. 7, for the local magnetization at the center of the chain].

Note that, close to $h_{\rm tr}(L)$, there are only two relevant levels (those whose energy difference becomes exponentially small) and therefore we can again apply a two-level truncation of the state space to compute the FSS functions. For the energy gap we recover Eq. (13), apart from a trivial but unique renormalization of the argument, $y = c\,x$, i.e.,

$$\mathcal{D}_f(y) = \mathcal{D}_{2l}(y/c), \tag{27}$$

where $\mathcal{D}_{2l}$ is the function obtained by the two-level truncation, cf. Eq. (13). This is once more supported by the data shown in Fig. 6, which nicely fit the two-level scaling behavior (with $c \approx 1.18$ for $g = 0.5$, and $c \approx 1.4$ for $g = 0.8$). This confirms that, even for EFBC, the FOQT is characterized by the crossing of two quantum energy levels.

For the magnetization we should be more careful, as Eq. (14) has been derived under the assumption that the magnetization of the two states is ± 1, respectively. For the central magnetization, this assumption is satisfied, as can be seen from Fig. 7 [indeed $\mathcal{M}_{cf}(y)$ converges to ± 1, as $y \to \pm\infty$], and hence we expect

$$\mathcal{M}_{cf}(y) = \mathcal{M}_{2l}(y/c), \tag{28}$$

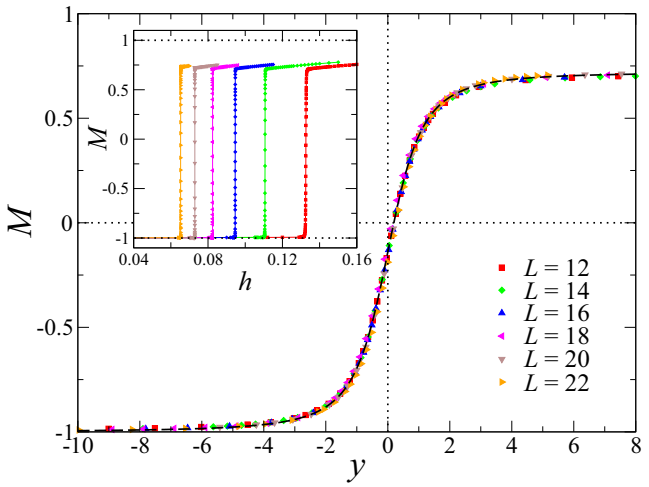

FIG. 8. Average magnetization M, as a function of the scaling variable y, for several system sizes (see the legend) and $g = 0.5$. We also report (continuous black curve) the two-level prediction (29), where the constant c is the same as in Fig. 6. In the inset we report M as a function of h.

with $\mathcal{M}_{2l}$ given in Eq. (14), and the same constant c obtained in the analysis of the gap. The results shown in Fig. 7 are fully consistent. On the other hand, the assumption is not true for the average magnetization M. Indeed, for $y \to \infty$, it converges to a value that is less than 1—see the inset of Fig. 8. We can identify this value with the magnetization M_{2s} of the ground state that is obtained by approaching $h_{\rm tr}(L)$ from above and is the relevant one in the limit $y \to \infty$. Numerically, we find $M_{2s} \approx 0.72$ and $M_{2s} \approx 0.52$ for $g = 0.5$ and $g = 0.8$, respectively. Using the two-level truncation, we predict for the scaling function

$$\mathcal{M}_f(y) = \mathcal{M}_{2l,a}(y/c),$$
$$\mathcal{M}_{2l,a}(x) = \frac{M_{2s}-1}{2} + \frac{M_{2s}+1}{2}\frac{x}{\sqrt{1+x^2}}, \tag{29}$$

which interpolates between $\mathcal{M}_{2l,a}(x \to -\infty) = -1$ and $\mathcal{M}_{2l,a}(x \to \infty) = M_{2s}$. Numerical results are in perfect agreement—see Fig. 8 for the data at $g = 0.5$.

It is important to note that the energy difference between the ground state and the higher excited states is expected to be of order h, hence of order $1/L$ at the transition point. The presence of this tower of states does not contradict the validity of the two-level approximation, since the relevant ratios $\Delta(L)/\Delta_{0,n}(L)$ vanish exponentially for all $n \geqslant 2$.

An interesting question concerns the nature of the two states which give rise to the above level-crossing scenario in the large L limit. One of them is the ground state for $h = 0$, i.e., the negatively magnetized state with $M = -1$ in the large-L limit; the other one is a state with a large positively magnetized region around the center, and two negatively magnetized regions at the boundaries, separated by a kink and an antikink close to the left and right boundary, respectively—see, e.g., Fig. 1. Close to the transition, the size of such regions at the boundaries must be of order L, to guarantee that the average magnetization is strictly less than 1.

C. Large-h region

We now discuss the main features of the finite-size behavior for $h > h_{\rm tr}$. As stated above, in this regime, low-energy states are characterized by a positively magnetized region around the center of the chain and by two negatively magnetized regions at the boundaries. The nature of the central region can be easily understood by considering the central magnetization M_c, displayed in Fig. 9. As L increases, results rapidly approach a function of h only. This trivial dependence on h is expected, since M_c is a local quantity which is not sensitive to the boundaries. On the other hand, as we shall see below, the behavior in proximity of the boundaries is more involved.

In Fig. 10 we report the magnetization profile close to one of the boundaries. The local magnetization differs from the value at the center, in a region of size ℓ_- close to $x = 0$. The region where M varies significantly shrinks as h increases, as expected. A detailed analysis of the data shows that ℓ_- has a nontrivial power-law dependence on h, for h large enough. Indeed, numerical results and a phenomenological theory for the magnetization profile in this regime—see Sec. III D—lead

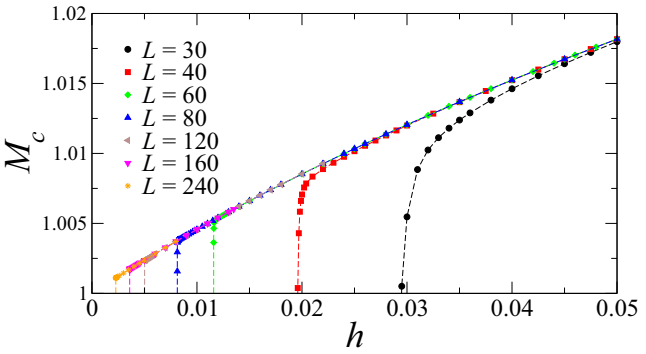

FIG. 9. The local central magnetization M_c in the large-h region, for fixed $g = 0.8$ and different system sizes, as indicated in the legend.

us to conjecture that

$$\ell_- \sim h^{-1/2}. \tag{30}$$

The emergence of this behavior is clearly supported by the plot reported in the inset of Fig. 10. If we plot the magnetization data versus $x\sqrt{h}$, we observe the collapse of the data. This is consistent with the data for a wide range of values of L and h, and for two different values of g. The scaling (30) implies that the relative size of the negatively magnetized region at one of the boundaries behaves as

$$v_- \equiv \frac{\ell_-}{L} \sim \frac{1}{h^{1/2}L}. \tag{31}$$

Equation (31) implies a scaling behavior for the average magnetization M, since this quantity is sensitive to the behavior at the boundaries. If we make a simple approximation in which the magnetization is -1 in two boundary regions of linear size ℓ_- and $+1$ in the central region of linear size $L - 2\ell_-$, we predict $M = 1 - 4\ell_-/L = 1 - 4v_-$. We can

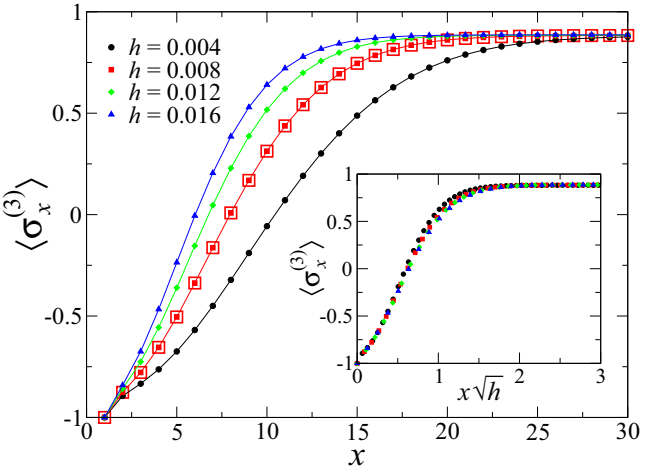

FIG. 10. Magnetization profile close to the boundaries, for $g = 0.8$ and several values of h, as indicated in the legend. Data are all for $L = 180$ (filled symbols), except empty red squares, which stand for $L = 100$ and $h = 0.008$ and are superposed to filled red squares (on the scale of the figure). The inset shows data collapse, after a rescaling of the x position by a factor $\sqrt{h}$.

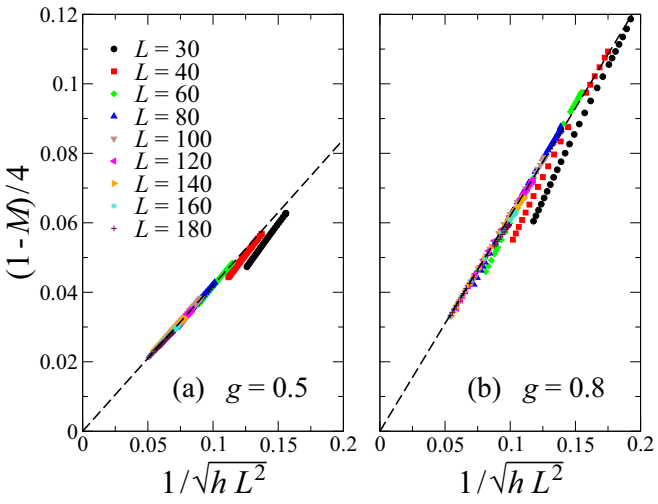

FIG. 11. Relative length $v_- = (1 - M)/4$ of the negatively magnetized phase, as a function of the rescaled variable $1/(h^{1/2}L)$. The various data sets are for different system sizes L, while the two panels are for $g = 0.5$ (a) and for $g = 0.8$ (b). Dashed straight lines are constrained fits of the numerical data at large L to Eq. (32).

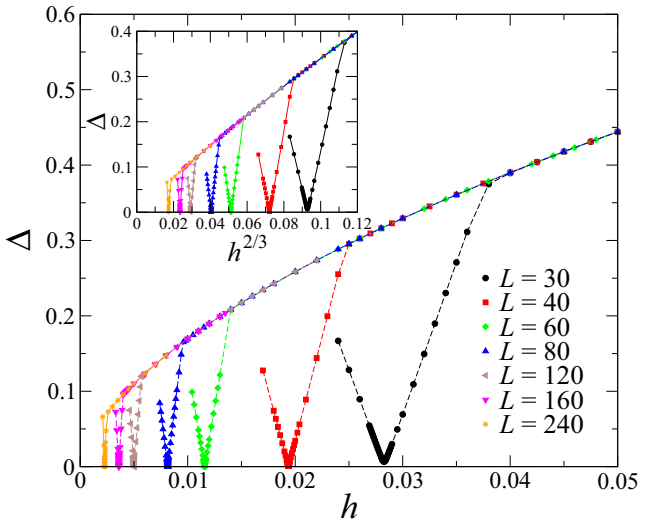

FIG. 12. Energy gap $\Delta(L, h)$ versus h in the large-h region, for $g = 0.8$ and different system sizes, as indicated in the legend. The inset displays the same data versus $h^{2/3}$. The dependence $\Delta \sim h^{2/3}$, see Eq. (34), emerges quite clearly.

take this equation as the definition of the relative length of the region in which the magnetization is negative. Equation (31) then predicts

$$v_- = \frac{1 - M}{4} \approx \frac{a(g)}{h^{1/2}\,L}, \tag{32}$$

for $h > h_{\rm tr}(L)$. This scaling behavior is clearly supported by the data displayed in Fig. 11, for two different values of g. We estimate $a(g = 0.5) \approx 0.42$ and $a(g = 0.8) \approx 0.62$ (see dashed straight lines in the figure). Therefore, Eq. (31) signals the presence of two negatively magnetized regions, whose width widens as h decreases at fixed L. However, since the scaling applies only up to $h_{\rm tr}(L)$, at fixed L, the width v_- satisfies

$$v_- \leqslant v_{\rm max} = \frac{a(g)}{h_{\rm tr}(L)^{1/2}\,L} \sim L^{-1/2}, \tag{33}$$

i.e., the maximum relative size decreases with L. Note that v_- decreases with increasing L only outside the transition region close to $h_{\rm tr}(L)$. In the scaling region around $h_{\rm tr}(L)$, v_- remains finite as L increases.

Let us finally analyze the energy gap $\Delta(L, h)$ between the two lowest-energy states. Results are reported in Fig. 12. For each value of L, the gap shows three distinct behaviors. For small magnetic fields Δ decreases. At $h_{\rm tr}(L)$ it is essentially zero on the scale of the figure, then it increases sharply up to an L-dependent value $h_\times(L)$ [28]. Finally, for $h > h_\times(L)$ it follows an L-independent curve. In the latter regime, the gap behaves as

$$\Delta(L, h) \sim h^{2/3}, \tag{34}$$

as it appears neatly from the rescaling provided in the inset. Note that Eq. (34) is the expected behavior for kink-antikink states in an external longitudinal magnetic field—see, e.g., Refs. [29–31]. This confirms our conjecture that the general features of the low-energy properties for $h > h_{\rm tr}$ are related to states with positively and negatively magnetized regions separated by kinklike structures.

The scaling (34) explains the nonanalytic behavior of $h_{\rm tr}(L)$, outlined in Eq. (22). Indeed, assume that the negatively magnetized state has an energy that scales as $E_{\rm magn} \approx E_0(L) - a_m hL - b_m h$, while all kink-antikink states have an energy that, consistently with the result (34), scales as $E_{\rm kink} = E_1(L) + a_k hL + c_k h^{2/3} + b_k h$. Equating the two energies, $E_{\rm magn} = E_{\rm kink}$, and taking into account that $E_1(L) - E_0(L)$ is finite for large L, we obtain the behavior (22), and in particular the $O(L^{-\xi})$ correction with $\zeta = 2/3$.

D. Phenomenological theory for the large-h region

We develop here a phenomenological theory for the behavior of the system. Given the numerical results, two states are relevant for the system. One should consider the negatively magnetized state $\mu(x) = -1$ of energy $E = hL$ (hereafter we adopt the shorthand notation $\mu(x) \equiv \langle \sigma_x^{(3)} \rangle$), which has average renormalized magnetization $M = -1$. The second relevant state is a double-kink state, characterized by two boundary regions of size ξ in which the magnetization is less than 1, and by one central region of size $L - 2\xi$ in which $\mu(x) = 1$. The average magnetization of the double-kink state is

$$M = \frac{1}{L}(L - a_1 \xi), \tag{35}$$

where a_1 is an appropriate constant. Correspondingly, its energy is

$$E = E_0 - hLM = E_0 - hL + a_1 \xi h, \tag{36}$$

where E_0 is the energy of the state in the absence of magnetic field. To compute E_0 we use a phenomenological approach. We assume that, for $h = 0$, the Hamiltonian can be written in

terms of $\mu(x)$ as

$$H = \int_0^L dx \left\{ a\left[\frac{d\mu(x)}{dx}\right]^2 + b[\mu(x)^2 - 1]^2 \right\}. \quad (37)$$

Boundary conditions require $\mu(0) = -1$ and $\mu(L) = -1$. The double-kink state can be parametrized as

$$\mu(x) = A\tanh[Bx] + A\tanh[B(L-x)] + C, \quad (38)$$

where C should be fixed to guarantee the boundary conditions. Equation (38) holds only if the localized kink and antikink do not interact, which in turn requires that $BL \gg 1$. If we further assume that $\mu(L/2) = 1$, then the profile can be written as

$$\mu(x) = 2\tanh[Bx] + 2\tanh[B(L-x)] - 3. \quad (39)$$

It is clear that B should be identified with the parameter ξ defined before. A simple computation gives

$$H = \frac{1}{B}a_0 + a_2 B \quad \text{for } BL \gg 1, \quad (40)$$

with

$$a_0 = \frac{64}{3}(3\ln 2 - 2)b, \quad a_2 = \frac{16}{3}a. \quad (41)$$

Therefore, the energy of the double-kink state in a magnetic field is

$$E = a_0\xi + \frac{a_2}{\xi} - hL + ha_1\xi. \quad (42)$$

The ground-state energy is obtained by minimizing E with respect to ξ. We obtain

$$\xi = \left(\frac{a_0 + a_1 h}{a_2}\right)^{-1/2}, \quad (43)$$

and, correspondingly,

$$E = 2\sqrt{a_2(a_0 + a_1 h)} - hL, \quad (44)$$

$$M = 1 - \frac{a_1}{L}\left(\frac{a_2}{a_0 + a_1 h}\right)^{1/2}. \quad (45)$$

The double-kink state competes with the magnetized one with $\mu(x) = -1$. The transition between the corresponding large-h and small-h regimes, where the ground states are the double-kink and magnetized states, respectively, occurs for

$$h = h_{\rm tr} = \frac{(a_0 a_2)^{1/2}}{L}. \quad (46)$$

Close to $h_{\rm tr}$, ξ is a finite number. The behavior changes as h increases. If $a_1 h \gg a_0$ we find $\xi \sim h^{-1/2}$ which shows that the region in which $\mu(x) < 1$ shrinks as $h^{-1/2}$. Moreover,

$$H \approx -hL\left[1 - 2\left(\frac{a_1 a_2}{hL^2}\right)^{1/2}\right], \quad (47)$$

$$M \approx 1 - \left(\frac{a_1 a_2}{hL^2}\right)^{1/2}. \quad (48)$$

Corrections to scaling are functions of hL^2, in agreement with numerical results—see Fig. 11.

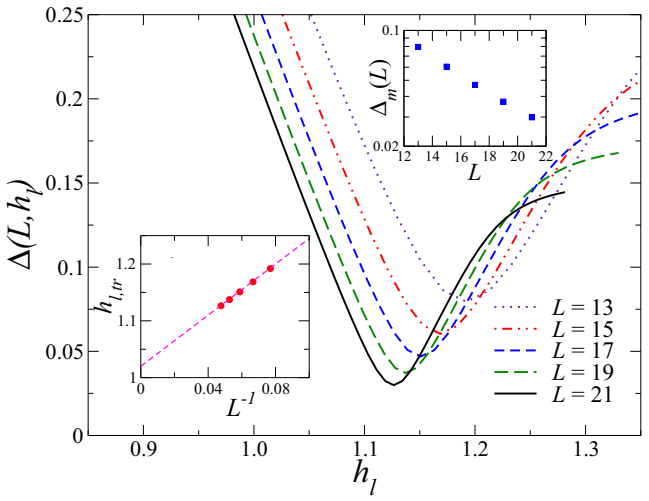

FIG. 13. The energy difference (gap) of the lowest states as a function of the localized magnetic field h_l at the center of the chain, for $g = 0.5$. The insets show its minimum $\Delta_m(L)$ (top inset) and the corresponding $h_{l,\rm tr}(L)$ (bottom inset), which appears to approach a constant value with $O(L^{-1})$ corrections. Indeed, by fitting the available data to $h_{l,\rm tr}(L) = h^*_{l,\rm tr} + b/L$, we obtain $h^*_{l,\rm tr} = 1.02$, see the dashed line in the corresponding inset.

E. Localized magnetic field

It is likewise interesting to discuss the case of an Ising chain with a localized magnetic field. To this purpose, let us consider a chain with an odd number of sites, $L = 2\ell + 1$, whose Hamiltonian is obtained by replacing the homogeneous term $-h\sum_{x=1}^{L}\sigma_x^{(3)}$ with a local term $-h_l\sigma_{x_c}^{(3)}$ in Eq. (17), where x_c is the central site. As in the homogeneous case, we can easily identify two distinct regions, in which ground-state properties are different. For small h_l, the system is magnetized, as before. For large h_l, it is enough to observe that, in the ground state, the central site is essentially fixed, as it should be aligned with the magnetic field. Therefore, the ground state is equivalent to that of two disjoint chains with fixed and opposite boundary conditions. Using the results of Refs. [9,19], we can conclude that the ground state is a kink state, with zero average magnetization. In this case the gap is [19]

$$\Delta(\ell) \approx \frac{3g}{1-g}\frac{\pi^2}{\ell^2}. \quad (49)$$

Thus, for h_l small and h_l large, the nature of the ground state differs. Therefore, we expect two different regions: a magnetized region for $h < h_{l,\rm tr}$ and a kink phase for $h > h_{l,\rm tr}$. For $h_l = h_{l,\rm tr}(L)$ a sharp transition occurs between the magnet and kink phases [19], where the magnetization profile is expected to qualitatively change. Its location $h_{l,\rm tr}(L)$ is expected to be associated with the minimum $\Delta_m(L)$ of the gap $\Delta(L, h_l)$, i.e., $\Delta_m(L) \equiv \Delta[L, h_{l,\rm tr}(L)]$.

This picture is confirmed by the numerical data, as shown in Fig. 13 for $g = 0.5$. As expected, $h_{l,\rm tr}(L)$ converges to a finite value for $L \to \infty$. For h_l close to such value, the

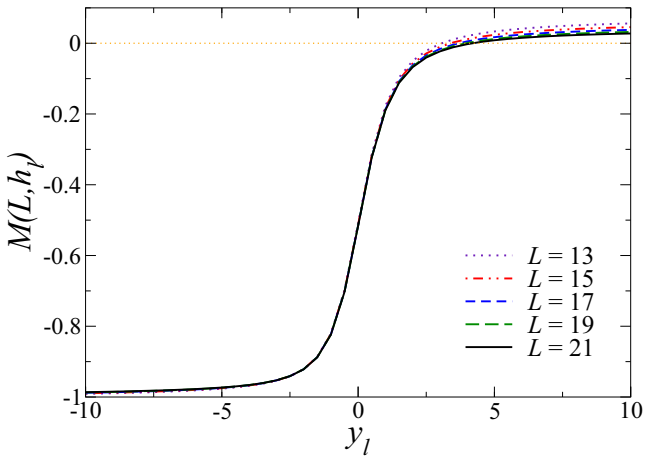

FIG. 14. Renormalized average magnetization $M(L, h_l)$ for $g = 0.5$ versus y_l [see Eq. (50)] for the model with a local magnetic field at the center of the chain. The curves appear to approach a scaling function $\mathcal{M}_l(y_l)$ with increasing L, i.e., $M(L \to \infty, h_l) \approx \mathcal{M}_l(y_l)$. Note that, although the magnetization appears positive for $y_l > 0$, its large-L limit is consistent with negative extrapolations, and $\mathcal{M}_l(y_l \to \infty) = 0$.

relevant FSS variable is expected to be

$$y_l = \frac{2m_0[h_l - h_{l,\mathrm{tr}}(L)]}{\Delta_m(L)}. \tag{50}$$

We note that, like for the case of the global magnetic field considered previously, the definition of the scaling variable y_l requires the actual values of $h_{l,\mathrm{tr}}(L)$ and $\Delta_m(L)$ for the size L, and not their asymptotic behaviors. Then, in the large-L limit, we expect that

$$M(L, h) \approx \mathcal{M}_l(y_l). \tag{51}$$

The scaling function $\mathcal{M}_l(y_l)$ is expected to be negative, and asymptotically $\mathcal{M}_l(y_l \to \infty) = 0$. The numerical data in Fig. 14 clearly support this scaling behavior. Qualitatively, we therefore obtain the same behavior as in the homogeneous case. Quantitatively, however, there are important differences. For instance, in the large-h_l region (i.e., for $h_l \gg h_{l,\mathrm{tr}}$), the average magnetization is smaller than 1 and correspondingly the size ℓ_- of the negatively magnetized region at the boundaries is of order L, and not of order $L^{1/2}$.

F. Summary

Our numerical results show that the quantum Ising chain with EFBC favoring one of the magnetized phases develops notable scaling features along the FOQT line. The FSS arising from the interplay between the size L and the bulk longitudinal field h turns out to be intriguingly more complex than that observed with neutral boundary conditions, see in particular Sec. II B for PBC and OBC. In the case of EFBC with both ends favoring the same phase, the observables around $h = 0$ depend smoothly on h, up to a pseudo transition value $h_{\mathrm{tr}}(L)$, behaving as $h_{\mathrm{tr}}(L) \approx \eta/L$, where they develop a singularity. This corresponds to a sharp transition to the oppositely magnetized phase, which appears to be analogous to a discontinuous transition. Around the finite-size transition point $h_{\mathrm{tr}}(L)$, the system develops a FSS controlled by an exponentially vanishing gap $\Delta(L) \sim e^{-bL}$. The scaling arises from the competition of the two lowest-energy states, indeed, scaling functions correspond to those of a two-level system. The relevant low-energy states are superpositions of a negatively magnetized state, which is the ground state for $h < h_{\mathrm{tr}}(L)$, and of a state with a positively magnetized region around the center and two negatively magnetized regions at the boundaries, separated by kink-like structures (see the magnetization profile shown in Fig. 1). The latter state becomes the ground state for $h > h_{\mathrm{tr}}$. Outside the transition region, it is characterized by two negatively magnetized regions close to the boundaries, of typical size $\ell_- \sim h^{-1/2}$.

The classical counterpart of this complex scenario for quantum many-body systems at FOQTs has been investigated at thermal first-order transitions in statistical systems with disordered boundary conditions [32], where the interplay between the temperature and the finite size gives rise to a complex scenario as well, characterized by different scaling regions.

We also considered the case of a localized external longitudinal field. Again we can identify two different regimes separated by a transition at a finite value of the local magnetic field. However, at variance with what happens in the case of PBC and OBC (see the discussion in Sec. II B), the nature of the transition and of the high local-field phase differs. In particular, its FSS at the transition does not arise from an avoided two-level crossing in finite systems, and the average magnetization cannot exceed $M = 0$.

IV. CONCLUSIONS

We have investigated FSS at FOQTs when boundary conditions favor one of the two phases. We have shown that substantial differences emerge with respect to neutral boundary conditions, such as PBC.

For this purpose, we presented a numerical study of one of the simplest paradigmatic quantum many-body systems exhibiting a nontrivial zero-temperature behavior: the one-dimensional quantum Ising chain in the presence of a transverse field, whose zero-temperature phase diagram features a line of FOQTs driven by a longitudinal external field. We provided evidence that the interplay between the size L and the bulk longitudinal field h is more complex than that observed with neutral boundary conditions. In the case of EFBC favoring the same phase, for small values of h, observables depend smoothly on h, up to $h_{\mathrm{tr}}(L) \approx \eta/L$, where η is a g-dependent constant, where a sharp transition to the oppositely magnetized phase occurs. In proximity of $h_{\mathrm{tr}}(L)$, a universal FSS behavior emerges from the competition of the two lowest-energy states, separated by a gap which vanishes exponentially with L. For even larger longitudinal fields, $h > h_{\mathrm{tr}}(L)$, a scaling behavior controlled by another variable $\sim 1/(h^{1/2}\, L)$ appears.

We believe that analogous behaviors can be observed in other FOQTs, when boundary conditions favor one of the two phases. In particular, they should also occur in systems defined in more than one dimension. It would be also interesting to verify whether these complex behaviors may occur in FOQTs driven by even perturbations as well, where OBC favor the disordered phase and EFBC the ordered one. Some results

for the quantum Potts chain appeared in Ref. [16], where, however, only the behavior around $h = 0$, analogous to that discussed in Sec. III A, was considered.

Finally we mention that it would be tempting to generalize the discussion to off-equilibrium dynamics across the FOQT. For example, one could address a situation where the longitudinal field is subject to a time-dependent driving, and devise suitable scaling laws which may depend on the properties of the equilibrium transition [33], in analogy to what has been done so far for the same system with neutral boundary conditions [24]. However, in view of the presence of several different equilibrium scaling behaviors, the off-equilibrium dynamics in the presence of EFBC may exhibit an intriguing, and possibly more complex, scenario.

Quite remarkably, the FSS behavior outlined in this paper can be observed for relatively small sizes: in some cases a limited number of spins already displays the asymptotic behavior. Therefore, even systems of modest size ($L \lesssim 100$) may show definite signatures of the scaling laws derived in this work. In this respect, present-day quantum-simulation platforms have already demonstrated their capability to reproduce and control the dynamics of quantum Ising-like chains with a small number of spins. Ultracold atoms in optical lattices [34,35], trapped ions [36–40], and Rydberg atoms [41] seem to be the most promising candidates where the emerging universality properties of the quantum many-body physics discussed here can be tested with a minimal number of controllable objects.

[1] S. L. Sondhi, S. M. Girvin, J. P. Carini, and D. Shahar, Continuous quantum phase transitions, Rev. Mod. Phys. **69**, 315 (1997).

[2] S. Sachdev, *Quantum Phase Transitions* (Cambridge University Press, Cambridge, 1999).

[3] M. Vojta, Quantum phase transitions, Rep. Prog. Phys. **66**, 2069 (2003).

[4] M. N. Barber, Finite-size scaling, in *Phase Transitions and Critical Phenomena*, C. Domb and J. L. Lebowitz (eds.) (Academic Press, London, 1983), Vol. 8, p. 145.

[5] *Finite Size Scaling and Numerical Simulations of Statistical Systems*, (ed.) V. Privman (World Scientific, Singapore, 1990).

[6] F. M. Gasparini, M. O. Kimball, K. P. Mooney, and M. Diaz-Avilla, Finite-size scaling of ^{4}He at the superfluid transition, Rev. Mod. Phys. **80**, 1009 (2008).

[7] M. Campostrini, A. Pelissetto, and E. Vicari, Finite-size scaling at quantum transitions, Phys. Rev. B **89**, 094516 (2014).

[8] K. Binder, Theory of first-order phase transitions, Rep. Prog. Phys. **50**, 783 (1987).

[9] M. Campostrini, J. Nespolo, A. Pelissetto, and E. Vicari, Finite-size Scaling at First-Order Quantum Transitions, Phys. Rev. Lett. **113**, 070402 (2014).

[10] V. Piazza, V. Pellegrini, F. Beltram, W. Wegscheider, T. Jungwirth, and A. H. MacDonald, First-order phase transitions in a quantum Hall ferromagnet, Nature (London) **402**, 638 (1999).

[11] T. Vojta, D. Belitz, T. R. Kirkpatrick, and R. Narayanan, Quantum critical behavior of itinerant ferromagnets, Ann. Phys. (Leipzig) **8**, 593 (1999).

[12] M. Uhlarz, C. Pfleiderer, and S. M. Hayden, Quantum Phase Transitions in the Itinerant Ferromagnet $ZrZn_2$, Phys. Rev. Lett. **93**, 256404 (2004).

[13] C. Pfleiderer, Why first order quantum phase transitions are interesting, J. Phys.: Cond. Matter **17**, S987 (2005).

[14] W. Knafo, S. Raymond, P. Lejay, and J. Flouquet, Antiferromagnetic criticality at a heavy-fermion quantum phase transition, Nat. Phys. **5**, 753 (2009).

[15] Conservation laws may give rise to crossings of the lowest energy levels even in finite systems. In some models, such as particle systems conserving the particle number at quantum transitions driven by the chemical potential, such level crossings give rise to periodic modulations of the FSS functions—see, e.g., M. Campostrini and E. Vicari, Quantum critical behavior and trap-size scaling of trapped bosons in a one-dimensional optical lattice, Phys. Rev. A **81**, 063614 (2010).

[16] M. Campostrini, J. Nespolo, A. Pelissetto, and E. Vicari, Finite-size scaling at first-order quantum transitions of quantum Potts chains, Phys. Rev. E **91**, 052103 (2015).

[17] M. Campostrini, A. Pelissetto, and E. Vicari, Quantum transitions driven by one-bond defects in quantum Ising rings, Phys. Rev. E **91**, 042123 (2015).

[18] A. Pelissetto, D. Rossini, and E. Vicari, Dynamic finite-size scaling after a quench at quantum transitions, Phys. Rev. E **97**, 052148 (2018).

[19] M. Campostrini, A. Pelissetto, and E. Vicari, Quantum Ising chains with boundary fields, J. Stat. Mech. (2015) P11015.

[20] L. Bogani and W. Wernsdorfer, Molecular spintronics using single-molecule magnets, Nat. Mater. **7**, 179 (2008).

[21] A. L. Gaunt, T. F. Schmidutz, I. Gotlibovych, R. P. Smith, and Z. Hadzibabic, Bose-Einstein Condensation of Atoms in a Uniform Potential, Phys. Rev. Lett. **110**, 200406 (2013).

[22] P. Pfeuty, The one-dimensional Ising model with a transverse field, Ann. Phys. **57**, 79 (1970).

[23] G. G. Cabrera and R. Jullien, Role of boundary conditions in the finite-size Ising model, Phys. Rev. B **35**, 7062 (1987).

[24] A. Pelissetto, D. Rossini, and E. Vicari, Off-equilibrium dynamics driven by localized time-dependent perturbations at quantum phase transitions, Phys. Rev. B **97**, 094414 (2018).

[25] C. R. Laumann, R. Moessner, A. Scardicchio, and S. L. Sondhi, Quantum Adiabatic Algorithm and Scaling of Gaps at First-Order Quantum Phase Transitions, Phys. Rev. Lett. **109**, 030502 (2012).

[26] U. Schollwöck, The density-matrix renormalization group, Rev. Mod. Phys. **77**, 259 (2005).

[27] Since we are interested in the ground-state physics, the full diagonalization of the Hamiltonian matrix is not required. For this reason, we implemented a much faster Lanczos diagonalization technique for systems with up to $L = 22$ sites, corresponding to a Hilbert space of dimension $2^{22} \sim 4 \times 10^6$. For larger sizes, a standard finite-size DMRG algorithm enabled us to reach systems with few hundreds of sites using a limited amount of resources. We kept the truncation error below 10^{-8}, using a number of states up to $m \approx 400$.

[28] In the limit $g \to 0$, we can easily verify that $h_\times(L)$ scales as $1/L$. Our results for finite values of g are also consistent with this behavior.

[29] B. M. McCoy and T. T. Wu, Two-dimensional Ising field theory in a magnetic field: breakup of the cut in the two-point function, Phys. Rev. D **18**, 1259 (1978).

[30] R. Coldea, D. A. Tennant, E. M. Wheeler, E. Wawrzynska, D. Prabhakaran, M. Telling, K. Habicht, P. Smeibidl, and K. Kiefer, Quantum criticality in an Ising chain: Experimental evidence of the emergent E_8 symmetry, Science **327**, 177 (2010).

[31] S. B. Rutkevich, On the weak confinement of kinks in the one-dimensional quantum ferromagnet $CoNb_2O_6$, J. Stat. Mech. (2010) P07015.

[32] H. Panagopoulos, A. Pelissetto, and E. Vicari, Anomalous finite-size scaling at the thermal first-order transition of systems with disordered boundary conditions, arXiv:1805.04241.

[33] A. Chandran, A. Erez, S. S. Gubser, and S. L. Sondhi, Kibble-Zurek problem: Universality and the scaling limit, Phys. Rev. B **86**, 064304 (2012).

[34] I. Bloch, Quantum coherence and entanglement with ultracold atoms in optical lattices, Nature (London) **453**, 1016 (2008).

[35] J. Simon, W. S. Bakr, R. Ma, M. E. Tai, P. M. Preiss, and M. Greiner, Quantum simulation of antiferromagnetic spin chains in an optical lattice, Nature (London) **472**, 307 (2011).

[36] E. E. Edwards, S. Korenblit, K. Kim, R. Islam, M.-S. Chang, J. K. Freericks, G.-D. Lin, L.-M. Duan, and C. Monroe, Quantum simulation and phase diagram of the transverse-field Ising model with three atomic spins, Phys. Rev. B **82**, 060412(R) (2010).

[37] R. Islam, E. E. Edwards, K. Kim, S. Korenblit, C. Noh, H. Carmichael, G.-D. Lin, L.-M. Duan, C.-C. Joseph Wang, J. K. Freericks, and C. Monroe, Onset of a quantum phase transition with a trapped ion quantum simulator, Nat. Commun. **2**, 377 (2011).

[38] G.-D. Lin, C. Monroe, and L.-M. Duan, Sharp Phase Transitions in a Small Frustrated Network of Trapped Ion Spins, Phys. Rev. Lett. **106**, 230402 (2011).

[39] K. Kim, S. Korenblit, R. Islam, E. E. Edwards, M.-S. Chang, C. Noh, H. Carmichael, G.-D. Lin, L.-M. Duan, C. C. Joseph Wang, J. K. Freericks, and C. Monroe, Quantum simulation of the transverse Ising model with trapped ions, New J. Phys. **13**, 105003 (2011).

[40] S. Debnath, N. M. Linke, C. Figgatt, K. A. Landsman, K. Wright, and C. Monroe, Demonstration of a small programmable quantum computer with atomic qubits, Nature (London) **536**, 63 (2016).

[41] H. Labuhn, D. Barredo, S. Ravets, S. de Leseleuc, T. Macri, T. Lahaye, and A. Browaeys, Tunable two-dimensional arrays of single Rydberg atoms for realizing quantum Ising models, Nature (London) **534**, 667 (2016).